

1 **Novel genomic loci influence patterns of structural covariance in the human** 2 **brain**

3 **Supporting Information**

4
5 Junhao Wen^{1,2*}, Ilya M. Nasrallah^{2,3}, Ahmed Abdulkadir², Theodore D. Satterthwaite^{2,4}, Zhijian Yang²,
6 Guray Erus², Timothy Robert-Fitzgerald⁵, Ashish Singh², Aristeidis Sotiras⁶, Aleix Boquet-Pujadas⁷,
7 Elizabeth Mamourian², Jimit Doshi², Yuhan Cui², Dhivya Srinivasan², Ioanna Skampardonis², Jiong
8 Chen², Gyujoon Hwang², Mark Bergman², Jingxuan Bao⁸, Yogasudha Veturi⁹, Zhen Zhou², Shu Yang⁸,
9 Paola Dazzan¹⁰, Rene S. Kahn¹¹, Hugo G. Schnack¹², Marcus V. Zanetti¹³, Eva Meisenzahl¹⁴, Geraldo F.
10 Busatto¹³, Benedicto Crespo-Facorro¹⁵, Christos Pantelis¹⁶, Stephen J. Wood¹⁷, Chuanjun Zhuo¹⁸, Russell
11 T. Shinohara^{2,5}, Ruben C. Gur⁴, Raquel E. Gur⁴, Nikolaos Koutsouleris¹⁹, Daniel H. Wolf^{2,4}, Andrew J.
12 Saykin²⁰, Marylyn D. Ritchie⁹, Li Shen⁸, Paul M. Thompson²¹, Olivier Colliot²², Katharina Wittfeld²³,
13 Hans J. Grabe²³, Duygu Tosun²⁴, Murat Bilgel²⁵, Yang An²⁵, Daniel S. Marcus²⁶, Pamela LaMontagne²⁶,
14 Susan R. Heckbert²⁷, Thomas R. Austin²⁷, Lenore J. Launer²⁸, Mark Espeland²⁹, Colin L Masters³⁰, Paul
15 Maruff³⁰, Jurgen Fripp³¹, Sterling C. Johnson³², John C. Morris³³, Marilyn S. Albert³⁴, R. Nick Bryan³,
16 Susan M. Resnick²⁵, Yong Fan², Mohamad Habes³⁵, David Wolk^{2,36}, Haochang Shou^{2,5}, and Christos
17 Davatzikos^{2*}

18
19 ¹Laboratory of AI and Biomedical Science (LABS), Stevens Neuroimaging and Informatics Institute, Keck School of
20 Medicine of USC, University of Southern California, Los Angeles, California, USA.

21 ²Artificial Intelligence in Biomedical Imaging Laboratory (AIBIL), Center for Biomedical Image Computing and
22 Analytics, Perelman School of Medicine, University of Pennsylvania, Philadelphia, USA.

23 ³Department of Radiology, University of Pennsylvania, Philadelphia, USA.

24 ⁴Department of Psychiatry, Perelman School of Medicine, University of Pennsylvania, Philadelphia, USA

25 ⁵Penn Statistics in Imaging and Visualization Center, Department of Biostatistics, Epidemiology, and Informatics,
26 Perelman School of Medicine, University of Pennsylvania, Philadelphia, USA

27 ⁶Department of Radiology and Institute for Informatics, Washington University School of Medicine, St. Louis, USA

28 ⁷Biomedical Imaging Group, EPFL, Lausanne, Switzerland

29 ⁸Department of Biostatistics, Epidemiology and Informatics University of Pennsylvania Perelman School of Medicine,
30 Philadelphia, USA

31 ⁹Department of Genetics and Institute for Biomedical Informatics, Perelman School of Medicine, University of
32 Pennsylvania, Philadelphia, PA, USA

33 ¹⁰Department of Psychological Medicine, Institute of Psychiatry, Psychology and Neuroscience, King's College
34 London, London, UK

35 ¹¹Department of Psychiatry, Icahn School of Medicine at Mount Sinai, New York, USA

36 ¹²Department of Psychiatry, University Medical Center Utrecht, Utrecht, Netherlands

37 ¹³Institute of Psychiatry, Faculty of Medicine, University of São Paulo, São Paulo, Brazil

38 ¹⁴Department of Psychiatry and Psychotherapy, HHU Düsseldorf, Germany

39 ¹⁵Hospital Universitario Virgen del Rocío, University of Sevilla-IBIS; IDIVAL-CIBERSAM, Sevilla, Spain

40 ¹⁶Melbourne Neuropsychiatry Centre, Department of Psychiatry, University of Melbourne and Melbourne Health,
41 Carlton South, Australia

42 ¹⁷Orygen and the Centre for Youth Mental Health, University of Melbourne; and the School of Psychology,
43 University of Birmingham, UK

44 ¹⁸Key Laboratory of Real Time Tracing of Brain Circuits in Psychiatry and Neurology (RTBCPN-Lab), Nankai
45 University Affiliated Tianjin Fourth Center Hospital; Department of Psychiatry, Tianjin Medical University, Tianjin,
46 China

47 ¹⁹Department of Psychiatry and Psychotherapy, Ludwig-Maximilian University, Munich, Germany

48 ²⁰Radiology and Imaging Sciences, Center for Neuroimaging, Department of Radiology and Imaging Sciences,
49 Indiana Alzheimer's Disease Research Center and the Melvin and Bren Simon Cancer Center, Indiana University
50 School of Medicine, Indianapolis

51 ²¹Imaging Genetics Center, Mark and Mary Stevens Neuroimaging and Informatics Institute, Keck School of
52 Medicine of USC, University of Southern California, Marina del Rey, California

53 ²²Sorbonne Université, Institut du Cerveau - Paris Brain Institute - ICM, CNRS, Inria, Inserm, AP-HP, Hôpital de la
54 Pitié Salpêtrière, F-75013, Paris, France
55 ²³Department of Psychiatry and Psychotherapy, German Center for Neurodegenerative Diseases (DZNE), University
56 Medicine Greifswald, Germany
57 ²⁴Department of Radiology and Biomedical Imaging, University of California, San Francisco, CA, USA
58 ²⁵Laboratory of Behavioral Neuroscience, National Institute on Aging, NIH, USA
59 ²⁶Department of Radiology, Washington University School of Medicine, St. Louis, Missouri, USA
60 ²⁷Cardiovascular Health Research Unit and Department of Epidemiology, University of Washington, Seattle, WA,
61 USA
62 ²⁸Neuroepidemiology Section, Intramural Research Program, National Institute on Aging, Bethesda, Maryland, USA
63 ²⁹Sticht Center for Healthy Aging and Alzheimer's Prevention, Wake Forest School of Medicine, Winston-Salem,
64 North Carolina, USA
65 ³⁰Florey Institute of Neuroscience and Mental Health, The University of Melbourne, Parkville, VIC, Australia
66 ³¹CSIRO Health and Biosecurity, Australian e-Health Research Centre CSIRO, Brisbane, Queensland, Australia
67 ³²Wisconsin Alzheimer's Institute, University of Wisconsin School of Medicine and Public Health, Madison,
68 Wisconsin, USA
69 ³³Knight Alzheimer Disease Research Center, Washington University in St. Louis, St. Louis, MO, USA
70 ³⁴Department of Neurology, Johns Hopkins University School of Medicine, USA
71 ³⁵Glenn Biggs Institute for Alzheimer's & Neurodegenerative Diseases, University of Texas Health Science Center at
72 San Antonio, San Antonio, USA
73 ³⁶Department of Neurology and Penn Memory Center, University of Pennsylvania, Philadelphia, USA
74
75 *Corresponding authors:
76 Junhao Wen, Ph.D. – junhaowe@usc.edu
77 2025 Zonal Ave, Los Angeles, CA 90033, United States
78 Christos Davatzikos, Ph.D. – Christos.Davatzikos@pennmedicine.upenn.edu
79 3700 Hamilton Walk, 7th Floor, Philadelphia, PA 19104, United States
80

81 **eText 1: Sensitivity check analysis for the GWAS using PSC C32_1**
82 **eText 2: Institutional Review Board (IRB) statement**
83 **eText 3: The four datasets and populations defined in this study**
84 **eMethod 1: Empirical validation of sopNMF**
85 **eMethod 2: Reproducibility index**
86 **eMethod 3: Inter-site image harmonization**
87 **eMethod 4: Quality check of the image processing pipeline**
88 **eMethod 5 Definition of the index, candidate, independent significant, and SNP and**
89 **genomic locus**
90 **eMethod 6 Cross-validation procedure for PAML**
91 **eFigure 1: Comparison between opNMF and sopNMF**
92 **eFigure 2: Reproducibility of the sopNMF brain parcellation**
93 **eFigure 3: Scatter plot for the h^2 estimates from the discovery and replication sets**
94 **eFigure 4: Sensitivity check for the GWAS results using the discovery set in UKBB**
95 **eFigure 5: Machine learning performance for disease classification and age prediction**
96 **eFigure 6: Annotation of MUSE PSCs to MuSIC PSCs based on the overlap index**
97 **eFigure 7: Summary statistics of the multi-scale PSCs of MuSIC**
98 **eTable 1: Study cohort characteristics**
99 **eTable 2: Clinical phenotypes and diagnoses used in machine learning classification**
100 **eTable 3: Comparison of variants identified via MuSIC with other studies**
101 **eTable 4: Classification balanced accuracy for disease classification and effect size of these**
102 **imaging signatures**
103 **eTable 5: 119 MUSE gray matter regions of interest**
104 **eAlgorithm 1: Algorithm for sopNMF**
105

106 **eText 1: Sensitivity check analysis for the GWAS using PSC C32_1**

107 We used the GWAS results (233 significant SNPs in 5 genomic loci) of the first PSC in C32
108 (C32_1) from the UKBB discovery set to demonstrate this.

109 We replicated all the 233 significant SNPs in 5 genomic loci both at the nominal level ($-\log_{10}[\text{p-value}] > 1.31$), and the Bonferroni corrected p-value threshold ($-\log_{10}[\text{p-value}] > 3.67$)
110 using the combined discovery and replication sets ($N=33,541$) (**SI eFigure 4b**), the 20,438
111 participants with all ancestries in the discovery set (**SI eFigure 4c**), and the 16,743 participants
112 in the discovery set with four additional imaging-related covariates (3 parameters for the brain
113 position in the lateral, longitudinal, and transverse directions, and 1 parameter for the head
114 motion from fMRI) (**SI eFigure 4d**). While replicating the results in 2386 participants with non-
115 European ancestries, we only replicated 41 SNPs (17.6%), passing the nominal significant
116 threshold (**SI eFigure 4e**). Finally, only 14 SNPs (6.4%) were replicated when replicating the
117 results using 1481 whole-genome sequencing (WGS) data from ADNI consolidated by the
118 AI4AD consortium¹⁶ (**SI eFigure 4f**). The low replication rates in other ancestries and
119 independent disease-specific populations are expected due to population stratification, disease-
120 specific effects, and reduced sample sizes. This further emphasizes the urge to enrich and
121 diversify genetic research with non-European ancestries and disease-specific populations.

123

124 **eText 2: Institutional Review Board (IRB) statement**

125 All individual studies were approved by their local corresponding Institutional Review Boards
126 (IRB). The iSTAGING and PHENOM consortia consolidated all individual imaging and clinical
127 data; imputed genotype data were directly downloaded from the UKBB website. Data from the
128 UKBB for this project pertains to application 35148. For iSTAGING, the IRB at the University
129 of Pennsylvania (protocol number: 825722) reviewed the research proposal on August 31st, 2016,
130 and updated it on August 31st, 2022. No human subjects were recruited or scanned. Existing de-
131 identified data will be used in this mega-analysis study pooling data from 17 studies: BLSA,
132 ADNI1, ADNI2, ADNI3, ACCORD-MIND, LookAhead, SPRINT, CARDIA, MESA, SHIP,
133 BIOCARD, WRAP, Penn-ADC, WHIMS-MRI, AIBL, OASIS, UKBB, MESA, HANDLS. For
134 PHENOM, the IRB at the University of Pennsylvania (protocol number: 828077) reviewed the
135 research proposal on August 19th, 2017. No human subjects were recruited or scanned. Existing
136 de-identified data will be used in this meta-analysis study pooling data from 10 studies at Penn,
137 Ludwick-Maximmilian University of Munich, Kings College-London, University of Utrecht,
138 University of Melbourne, University of Cantabria, University of Sao Paolo, Xijing Hospital
139 Shaanxi, Tianjin Anning Hospital, and Institute of Mental Health Peking University.

140

141 **eText 3: The four datasets and populations defined in this study**

142 We defined four populations or data sets per analysis across the paper: *i) discovery set, ii)*
143 *replication set, iii) training population, and iv) comparison population* (refer to **SI eText 2** for
144 details).

- 145 • Discovery set: It consists of a multi-disease and lifespan population that includes
146 participants from all 12 studies ($N=32,440$). Note that this population does not contain
147 the entire UKBB population but only our first download (July 2017, $N=21,305$).
- 148 • Replication set: We held 18,259 participants from the UKBB dataset to replicate the
149 GWAS results. We took these data from our second download of the UKBB dataset
150 (November 2021, $N=18,259$).
- 151 • Training population: We randomly drew 250 patients (PT), including AD, MCI, SCZ,
152 ASD, MDD, HTN (hypertension), DM (diabetes mellitus), and 250 healthy controls
153 (CN) per decade from the discovery set, ensuring that the PT and CN groups have
154 similar sex, study and age distributions. The resulting set of 4000 imaging data was used
155 to generate the MuSIC atlas with the sopNMF algorithm. The rationale is to maximize
156 variability across a balanced sample of multiple diseases or risk conditions, age, and
157 study protocols rather than overfit the entire data by including all images in training.
- 158 • Comparison population: To validate sopNMF compared to the original opNMF
159 algorithm, we randomly subsampled 800 participants from the training population (100
160 per decade for balanced CN and PT). For this scale of sample size, opNMF can load all
161 images into memory for batch learning.¹

162

163 **eMethod 1: Empirical validation of sopNMF.**

164 For the empirical validation of sopNMF, the comparison population (**Method 1** in the main
165 manuscript) was used so that the machine's memory could be sufficient to read the entire data for
166 opNMF. For sopNMF, different choices of batch size (i.e., BS=32, 64, 128, and 256) were
167 tested. We hypothesized that sopNMF could approximate the optima of opNMF during
168 optimization, i.e., resulting in similar parts-based representation, training loss, and sparsity.
169 TensorboardX was embedded into the sopNMF framework to monitor the training process
170 dynamically. All experiments were performed on an Ubuntu machine with a maximum RAM of
171 32 GB and 8 CPUs. The predefined maximum number of epochs for all experiments is 50,000,
172 and the tolerance of early stopping criteria is 100 epochs based on the training loss.

173 We qualitatively compared the extracted PSCs and quantitatively for the training loss, the
174 sparsity of the component matrix W , and the memory consumption for $C=20$ (number of PSCs).
175 The 20 PSCs were spatially consistent between opNMF and sopNMF, despite that some regions
176 were decomposed into different PSCs (i.e., the white ellipse in **eFig. 1A**). For the training loss,
177 opNMF obtained the lowest loss (1.103×10^6), and the loss of sopNMF were 1.107×10^6 , 1.108
178 $\times 10^6$, 1.111×10^6 and 1.210×10^6 for BS =256, 128, 64, and 32, respectively (**eFig. 1D**). For the
179 sparsity of the component matrix, all models obtained comparable results (sparsity ≈ 0.83 , **eFig.**
180 **1E**). The estimated memory consumptions during the training process were 28.65, 4.02, 3.81,
181 2.60, 1.47 GB for opNMF and sopNMF (BS =256, 128, 64, and 32), respectively
182 (**Fig. e1F**).

183

184 **eMethod 2: Reproducibility index.**

185 We proposed a reproducibility index (RI) to test the reproducibility of sopNMF for brain

186 parcellation:

- 187 • We used the Hungarian match algorithm² to match the pairs of PSCs between two splits
188 under the specific condition that maximizes the similarity (i.e., minimizes the cost of
189 workers/jobs in its original formulation).
- 190 • For each pair of PSCs, we calculated the inner product of the vectors (R^d), referred to as
191 RI. This index takes values between [0, 1], with higher values indicating higher
192 reproducibility.
- 193 • For each scale C , we presented the mean/standard deviation of the RIs for all PSCs.

194

195

196

197 **eMethod 3: Inter-site image harmonization**

198 We used an extensively validated statistical harmonization approach, i.e., ComBat-GAM,³ to
199 harmonize the extracted multi-scale PSCs. This method estimates the variability in volumetric
200 measures due to differences in site/cohort-specific imaging protocols based on variances observed
201 within and across control groups while preserving normal variances due to age, sex, and
202 intracranial volume (ICV) differences. The model was initially trained on the discovery set and
203 then applied to the replication set.

204

205 **eMethod 4: Quality check of the image processing pipeline.**

206 Raw T1-weighted MRIs were first quality checked (QC) for motion, image artifacts, or restricted
207 field-of-view. Another QC was performed: First, the images were examined by manually
208 evaluating for pipeline failures (e.g., poor brain extraction, tissue segmentation, and registration
209 errors). Furthermore, a second step automatically flagged images based on outlying values of
210 quantified metrics (i.e., PSC values); those flagged images were re-evaluated.

211

212 **eMethod 5: Definition of the index, candidate, independent significant, and lead SNP and**
213 **genomic locus.**

214 *Index SNP*

215 They are defined as SNPs with a p-value threshold $\leq 5e-8$ (*clump-p1*) from GWAS summary
216 statistics.

217 *Independent significant SNP*

218 They are defined as the index SNPs, which are independent of each other (not in linkage
219 disequilibrium) with $r^2 \leq 0.6$ (*clump-r2*) within 250 kilobases (non-overlapping, *clump-kb*) away
220 from each other.

221 *Lead SNP and genomic loci*

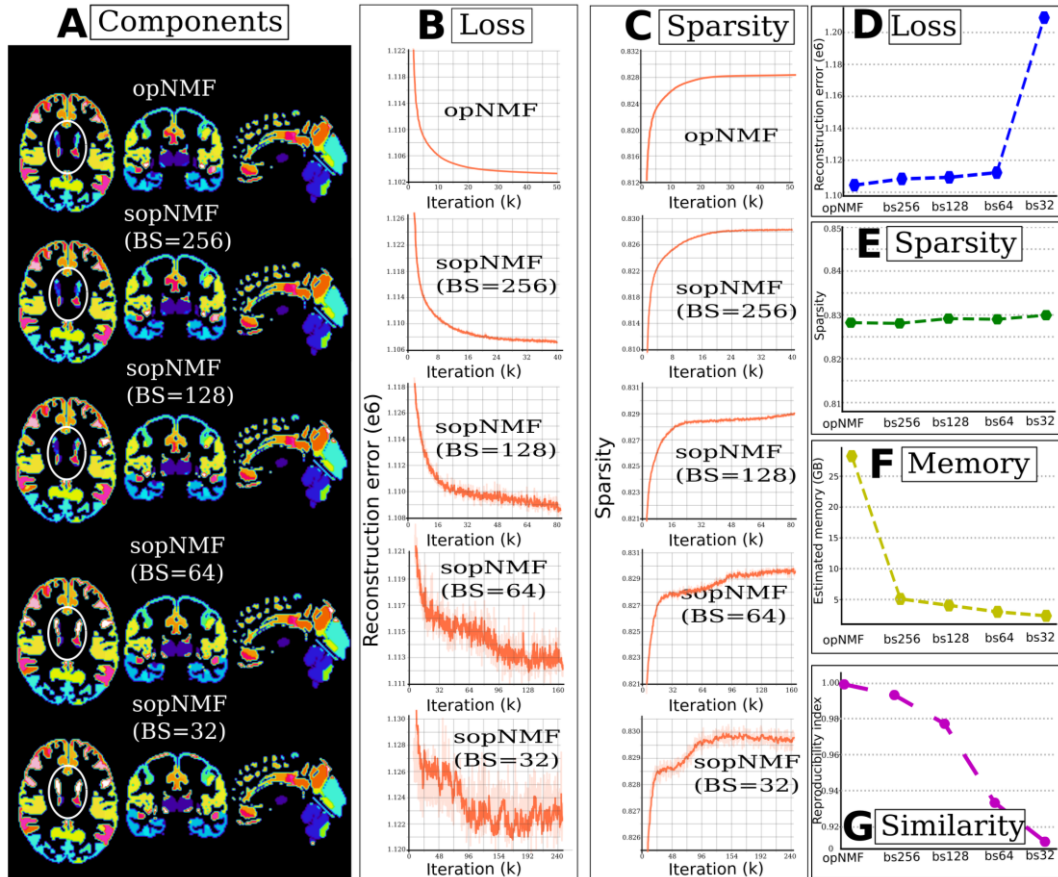
222 They are defined as the independent significant SNPs, which are independent of each other with
223 a more stringent $r^2 \leq 0.1$ (*clump-r2*) within 250 kilobases (non-overlapping, *clump-kb*) away
224 from each other. Each of these clumps is defined as a *genomic locus*.

225 *Candidate SNP*

226 With each genomic locus, candidate SNPs are defined as the SNPs whose association p-values
227 are smaller than 0.05 (*clump-p2*). The definitions followed instructions from FUMA⁴ and Plink⁵
228 software.

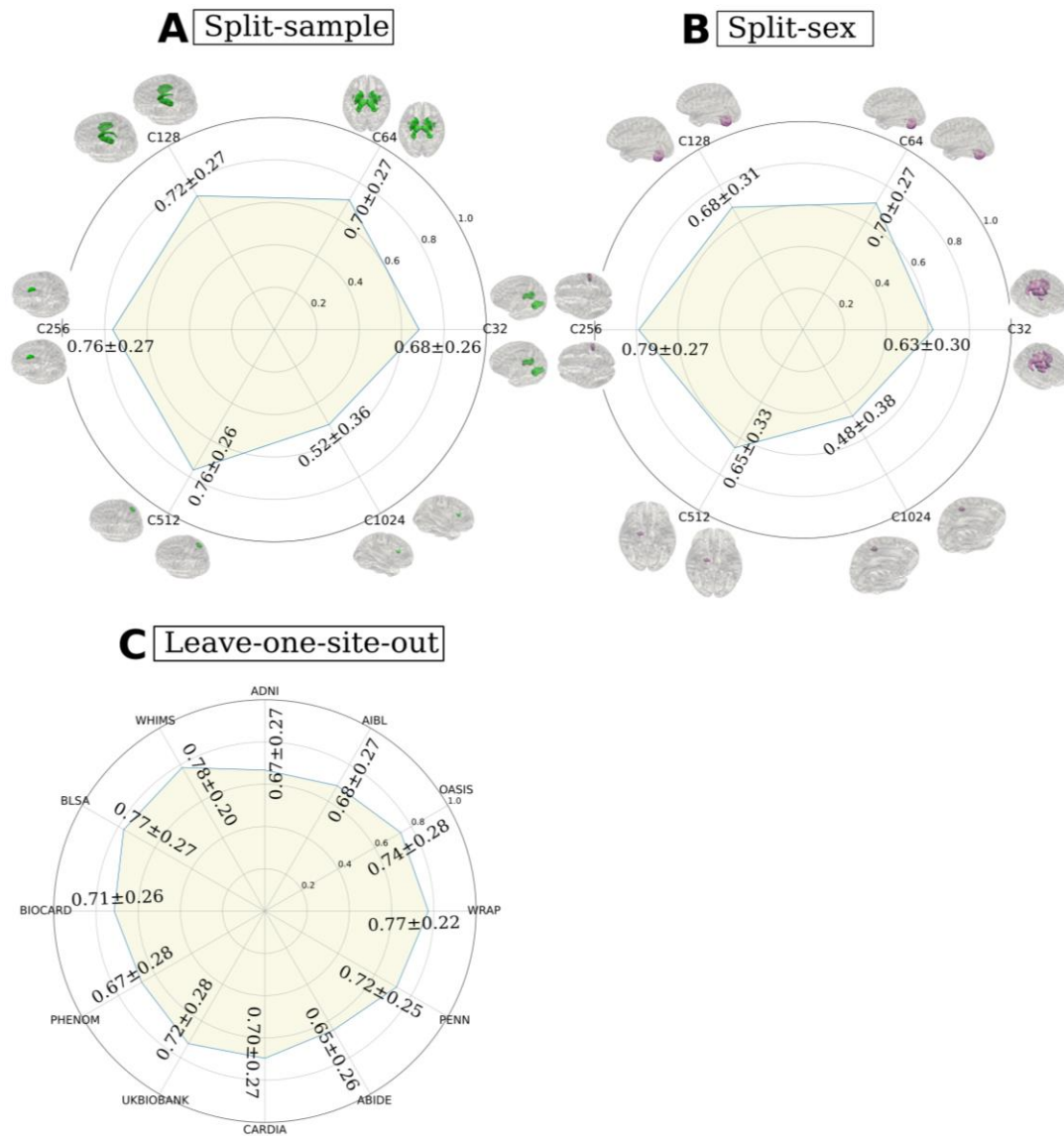
229 **eMethod 6: Cross-validation procedure for PAML.**

230 Nested cross-validation was adopted for all tasks following the good-practice guidelines
231 proposed in our previous works⁶⁻⁸. In particular, an outer loop was used to evaluate the task
232 performance (250 repetitions of random hold-out splits with 80% of data for training). In
233 contrast, an inner loop focused on tuning the hyperparameters (10-fold splits). We computed the
234 balanced accuracy (BA) to evaluate the classification tasks. We calculated the effect size
235 (Cohen's d) and p-value for each SPARE index to quantify its discriminative power.
236

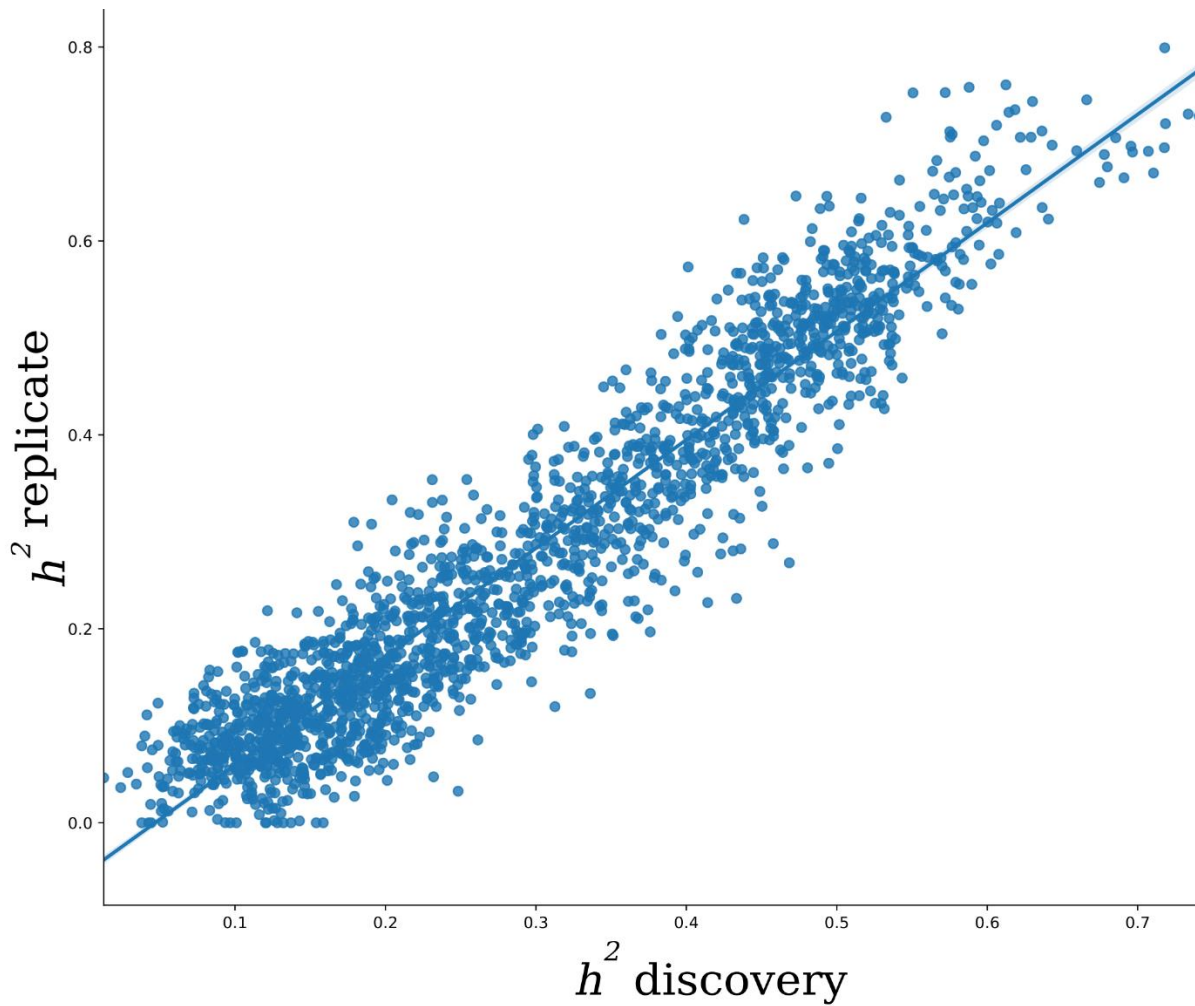


237
238
239
240
241
242
243
244

eFigure 1: Comparison between opNMF and sopNMF. (A) Qualitative evaluation: The extracted components are shown in the original image space, with each PSC displayed in a distinct color. The white ellipse indicates the region where the models diverge. Quantitative evaluation: training loss (B, D) and sparsity (C, E) demonstrated similar patterns between models, except that batch size (BS) = 32 had a larger loss than the other models. Comparing the estimated memory consumption during training across models shows significant advantages for all sopNMF models compared to opNMF.

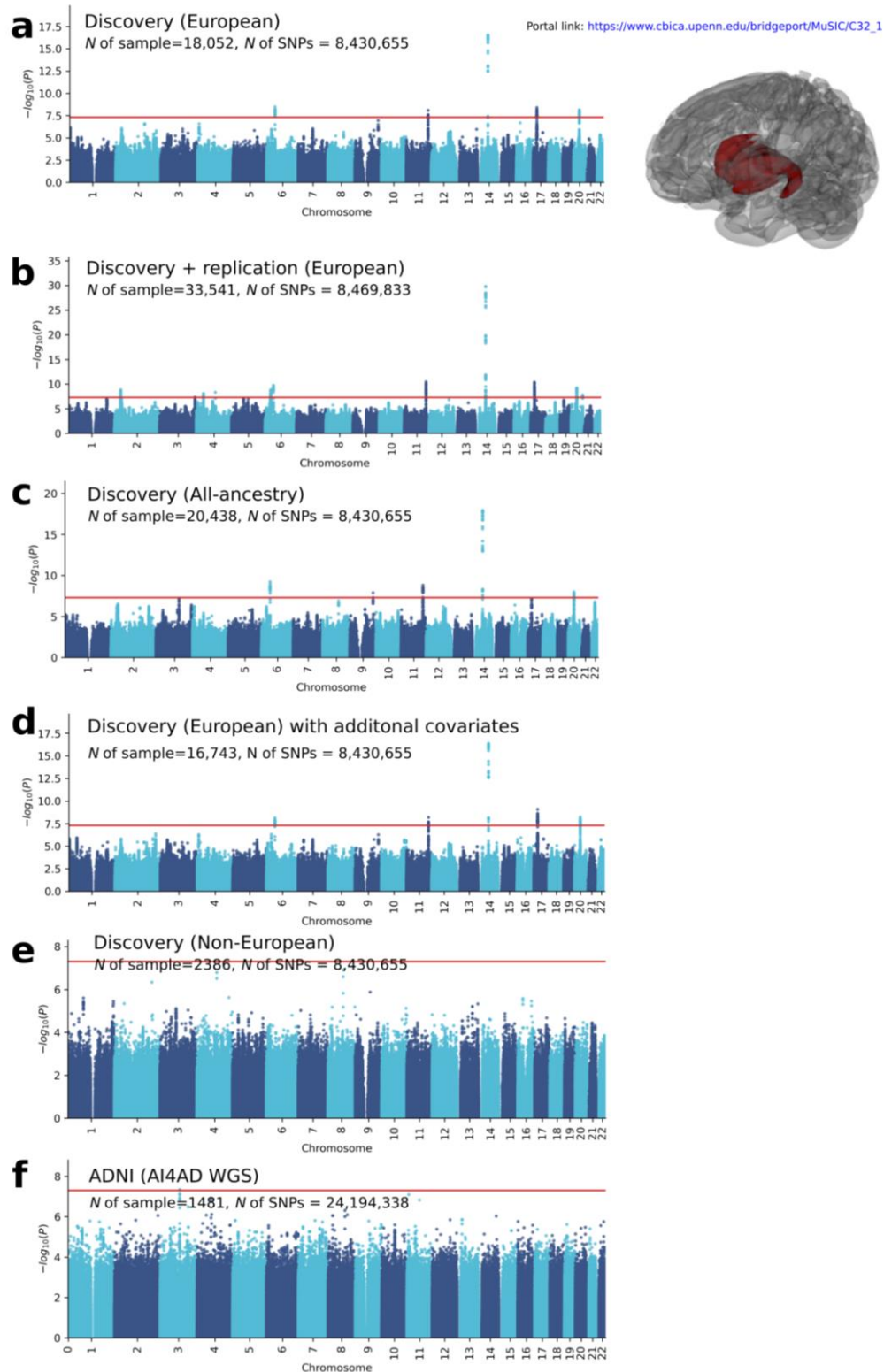


245
 246 **eFigure 2: Reproducibility of the sopNMF brain parcellation.** In general, sopNMF
 247 demonstrated high reproducibility under various conditions. For each brain PSC, the
 248 reproducibility index (RI) was calculated (**Supplementary eMethod 2**). (A) Split-sample
 249 analyses, where the training population ($N=4000$) was randomly split into two halves while
 250 maintaining similar age, sex, and site distribution between groups. (B) Split-sex
 251 analyses, where the training population was divided into males and females. Colored PSCs on the brain template
 252 illustrate the same PSC independently derived from the two splits. (C) Leave-one-site-out
 253 analyses for C32 PSCs., where the training populations excluding participants from each site
 254 (BIOCARD, ADNI, WARP, AIBL, ABIDE, BLSA, OASIS, CARDIA, PHENOM, PENN,
 255 UKBB, and WHIMS) were independently trained with sopNMF. The RI indices were compared
 256 to the sopNMF results using the full training sample ($N=4000$).
 257



259
260
261
262
263
264
265

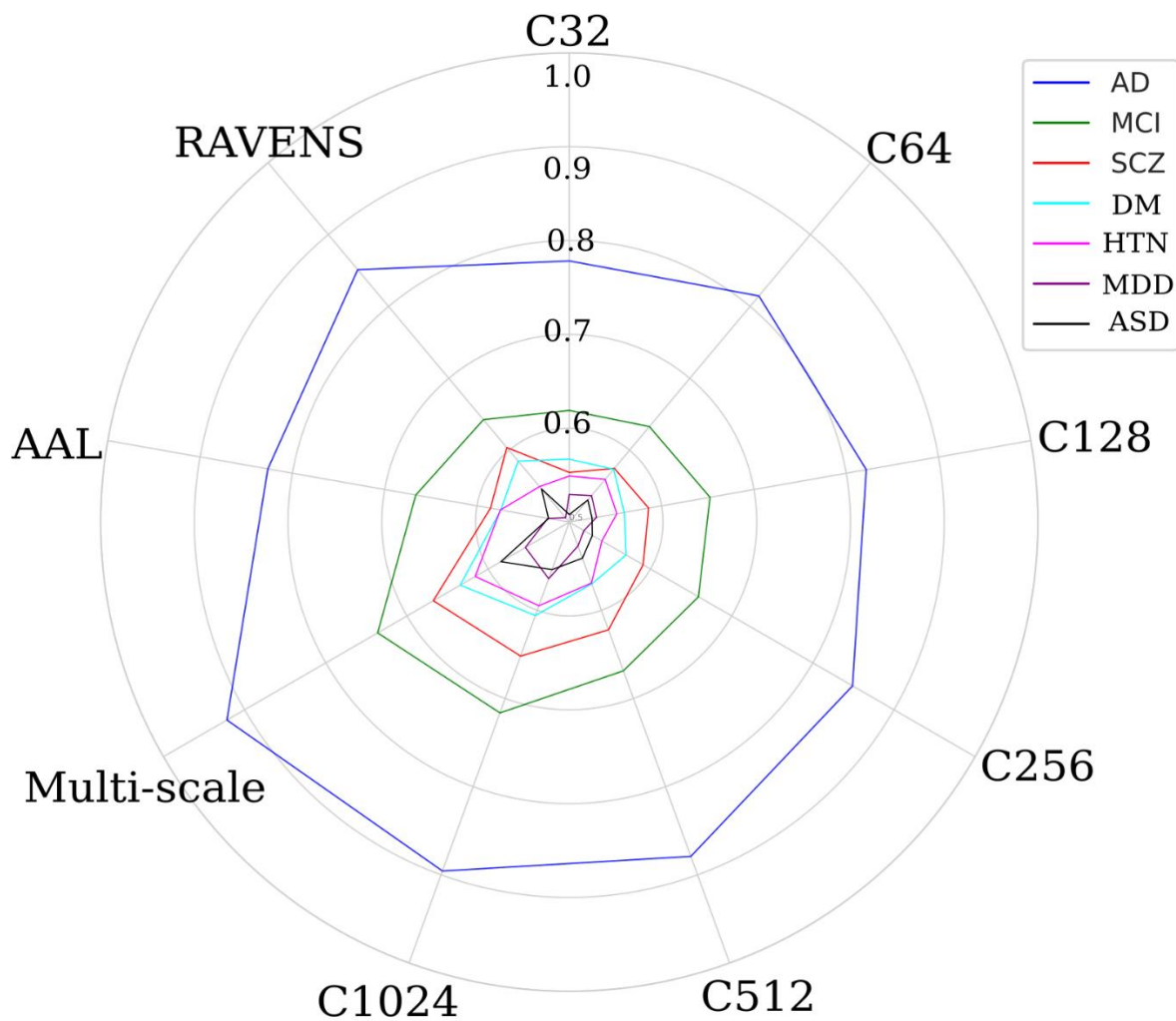
Figure 3: Scatter plot for the h^2 estimates from the discovery and replication sets. The SNP-based heritability was estimated independently for the discovery set ($N=18,052$) and replication set ($N=15,243$). In particular, the two estimates were highly correlated ($r = 0.94$, p -value $< 10^{-6}$), demonstrating a highly similar genetic architecture across different sets of UKBB data.



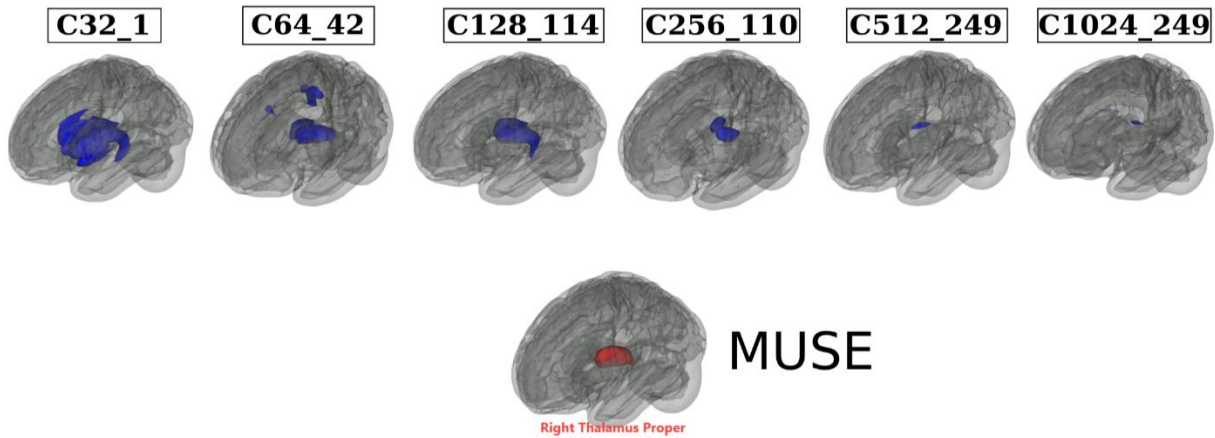
266
267
268
269
270

eFigure 4: Sensitivity check for the GWAS results using the discovery set in UKBB. **A)** The GWAS results for participants with European ancestry in the discovery set. **B)** The GWAS results for participants with European ancestry in the discovery and replication sets. **C)** The GWAS results for participants with all different ancestries in the discovery set. **D)** The GWAS

271 results for participants with European ancestry in the discovery set by adding four additional
272 imaging-related covariates. **E)** The GWAS results for participants with non-European ancestry in
273 the discovery set. **F)** The GWAS results for participants with the independent ADNI WGS data.



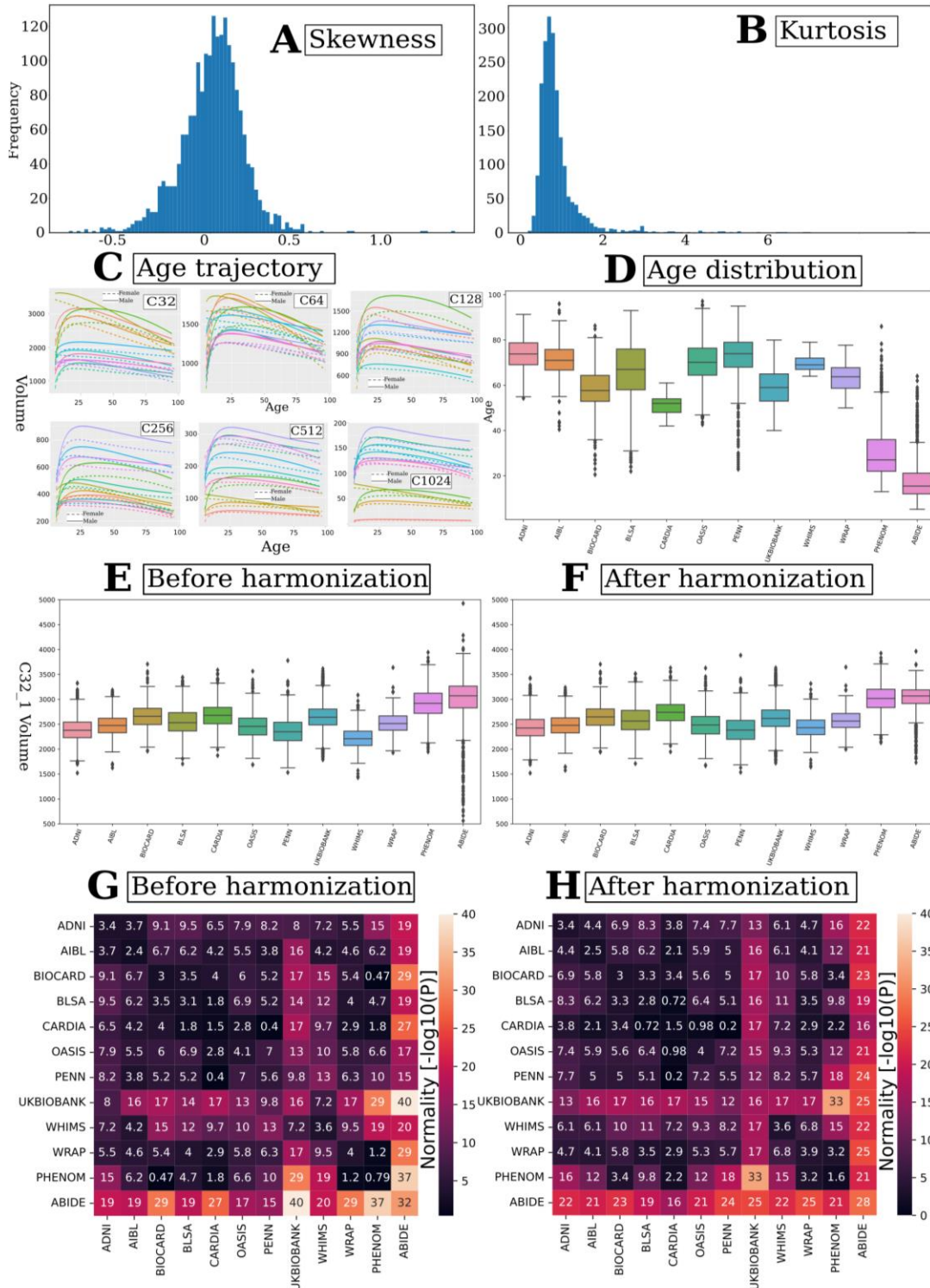
274
 275 **eFigure 5: Machine learning performance for disease classification.** Balanced accuracy (BA)
 276 for each classification task using different features from multi-scale MuSIC, AAL, and RAVENS
 277 (higher score better). Details are presented in **eTable 4**.
 278



279
280
281
282
283
284
285
286
287
288
289
290

eFigure 6: Annotation of MUSE ROIs to MuSIC PSCs based on the overlap index. We automatically annotated the 119 MUSE GM PSCs to the MuSIC atlases at all six scales ($C=32, 64, 128, 256, 512,$ and 1024). To this end, we calculated an overlap index (OI) to quantify the spatial overlaps between MUSE and MuSIC. For instance, for each MUSE PSC (**eTable 5**) vs. each of the 32 PSCs of MuSIC at $C=32$ scale, the OI equals the proportion of the number of overlap voxels and the total number of voxels in the MUSE PSC. Here we illustrate by mapping the right thalamus of MUSE to all 6 MuSIC atlases. The highest OIs are 0.82, 0.70, 0.86, 0.30, 0.09, 0.05 for C32_1, C64_42, C128_114, C256_110, C512_249, and C1024_249 PSCs. This functionality is available in BRIDGEPORT:

<https://www.cbica.upenn.edu/bridgeport/MUSE/Right%20Thalamus%20Proper>



291
 292 **eFigure 7: Summary statistics of the multi-scale PSCs of MuSIC.** Multi-scale PSCs show
 293 considerable normal distributions, i.e., symmetrical distribution (A) with a low kurtosis (B).
 294 Moreover, we fit the Generalized Additive Model for Location, Scale, and Shape (GAMLSS)⁹
 295 model (fractional polynomials with 2 degrees) to each PSC to delineate the age trajectory over
 296 the lifespan in males (solid lines) and females (dotted lines), respectively (C). For visualization

297 purposes, we selectively display the first 10 PSCs from each scale of the MuSIC atlases. In
298 general, males have larger brain volumes than females. For **D-F**, we selectively showed the
299 distribution of age (**D**) and the distribution of PSC volume before harmonization (**E**) and after
300 harmonization (**F**) for C32_1 within each site in the discovery set. For **G** and **H**, we tested the
301 normality of the PSC volume (C32_1) from each pair of sites using the Shapiro-Wilk test
302 (*scipy.stats.shapiro* function) in the discovery set before (**G**) harmonization and after
303 harmonization (**H**). A higher $-\log_{10}(P)$ indicates the data are less likely to be normally
304 distributed. As a general trend, our statistical harmonization techniques demonstrated a slight
305 improvement in the normality of the data. Additionally, we consistently applied normality
306 transformations to all statistical analyses, including GWAS, to mitigate any non-normality.
307

308 **eTable 1. Study cohort characteristics.**

309 The current study consists of two main populations/sets: the discovery set ($N=32,440$, including
 310 participants from the first download of the UKBB data) and the replication set ($N=18,259$, the
 311 second download of the UKBB data). To train the sopNMF model for MuSIC, we selected 250
 312 patients (PT) and 250 healthy controls (CN) for each decade of the discovery set, resulting in
 313 4000 participants in total, referred to as the training population. Age ranges from 5 to 97 years
 314 and is shown with mean and standard deviation. Sex is displayed with the number and
 315 percentage of female participants. Data was collected from 12 studies, 130 sites, and 12
 316 countries. The number of sites (country) per study is detailed as follows:

- 317 • ADNI: 63 sites (USA)
- 318 • UKBB: 5 sites (UK)
- 319 • AIBL: 2 sites (Australia)
- 320 • BIOCARD: 2 sites (USA)
- 321 • BLSA: 1 site (USA)
- 322 • CARDIA: 3 sites (USA)
- 323 • OASIS: 1 site (USA)
- 324 • PENN: 1 site (USA)
- 325 • WHIMS: 14 sites (USA)
- 326 • WRAP 1 site (USA)
- 327 • PHENOM: 12 sites (China, Brazil, Australia, Germany, Spain, USA, Netherlands)
- 328 • ABIDE: 25 sites (USA, Netherlands, Belgium, Germany, Ireland, Switzerland, France)

329 Abbreviations: CN: healthy control; AD: Alzheimer's disease; MCI: mild cognitive impairment;
 330 SCZ: schizophrenia; ASD: autism spectrum disorder; MDD: major depressive disorder; DM:
 331 diabetes; HTN: hypertension.

332 ^aUKBB data were separately downloaded two times: the first was the $N=21,305$ in the discovery
 333 set, and the second was the replication set.

334 ^bWe define CN (healthy controls) as participants that do not have any of the diseases listed here.
 335 These CN participants might have diagnoses of other illnesses or comorbidities (e.g., participants
 336 from UKBB have a wide range of pathology based on ICD-10).

337

Study	N (50,699)	Age (5-97 year)	Sex (female/%)	CN ^b	AD	MCI	SCZ	ASD	MDD	DM	HTN
Discovery set	32,440	60.04± 14.87	16,868/52	24,980	954	1288	1094	597	1476	1093	958
ADNI	1765	73.66± 7.19	798/45	297	343	875	NA	NA	NA	NA	250
UKBB ^a	21,305	62.58± 7.48	10,101/53	18,735	1	NA	NA	NA	1476	1093	NA
AIBL	830	71.36± 6.78	471/57	625	86	115	NA	NA	NA	NA	4
BIOCARD	288	58.15± 10.54	115/60	283	1	4	NA	NA	NA	NA	NA
BLSA	1114	65.44± 14.11	589/53	729	9	11	NA	NA	NA	NA	365
CARDIA	892	51.21± 3.98	471/53	620	NA	NA	NA	NA	NA	NA	272
OASIS	983	69.92± 9.75	557/57	759	220	NA	NA	NA	NA	NA	4

PENN	807	72.63± 10.65	333/59	173	294	283	NA	NA	NA	NA	57
WHIMS	995	69.61± 3.64	995/100	986	NA	NA	NA	NA	NA	NA	6
WRAP	116	63.36± 6.06	79/68	116	NA	NA	NA	NA	NA	NA	NA
PHENOM	2125	30.21± 10.60	854/40	1031	NA	NA	1094	NA	NA	NA	NA
ABIDE	1220	17.92± 9.01	203/17	623	NA	NA	NA	597	NA	NA	NA
Replication set^a	18,259	54.70± 7.43	9742/53	NA	NA	NA	NA	NA	NA	NA	NA

338
339

340 **eTable 2: Clinical phenotypes and diagnoses used in machine learning classification.**

341 We harmonized the population of the phenotypes of interest per study definitions:

- 342 • We combined AD and MCI patients from ADNI, PENN, and AIBL but excluded OASIS
 343 subjects because of the different diagnostic criteria of an AD patient in OASIS.
 344 • For several binary disease phenotypes, we used the ICD-10 diagnosis
 345 (<https://biobank.ndph.ox.ac.uk/ukb/field.cgi?id=41270>). Note that ICD-10 diagnoses are
 346 generally collected from the participants' medical inpatient records. We first included
 347 diseases from the following categories:
- 348 ○ Diseases of the blood and blood-forming organs and certain disorders involving the
 349 immune mechanism (D-XXX, XXX represents the ID of a specific disease);
 - 350 ○ Endocrine, nutritional, and metabolic diseases (E-XXX);
 - 351 ○ Mental and behavioral disorders (F-XXX);
 - 352 ○ Diseases of the nervous system (G-XXX);
 - 353 ○ Diseases of the circulatory system (I-XXX).

354 We then set a threshold of 75 patients for any ICD-10 diagnosis. We finally randomly
 355 selected age and sex-matched healthy controls (excluding all patients in all diagnoses). ^a:
 356 For major depressive disorder, we used the inclusion criteria from our previous work.¹⁰

- 357 • For cognitive scores, we included:
- 358 ○ Tower rearranging (<https://biobank.ndph.ox.ac.uk/showcase/field.cgi?id=21004>)
 - 359 ○ Matrix pattern (<https://biobank.ndph.ox.ac.uk/showcase/field.cgi?id=6373>)
 - 360 ○ TMT-A (<https://biobank.ndph.ox.ac.uk/showcase/field.cgi?id=6348>)
 - 361 ○ TMT-B (<https://biobank.ndph.ox.ac.uk/showcase/field.cgi?id=6350>)
 - 362 ○ DSST (<https://biobank.ndph.ox.ac.uk/showcase/field.cgi?id=23324>)
 - 363 ○ Pairs matching (<https://biobank.ndph.ox.ac.uk/showcase/field.cgi?id=399>)
 - 364 ○ Numerical memory (<https://biobank.ndph.ox.ac.uk/showcase/field.cgi?id=4282>)
 - 365 ○ Prospective memory (<https://biobank.ndph.ox.ac.uk/showcase/field.cgi?id=4288>)
 - 366 ○ Reaction time (<https://biobank.ndph.ox.ac.uk/showcase/field.cgi?id=20023>)
 - 367 ○ Fluid intelligence (<https://biobank.ndph.ox.ac.uk/showcase/field.cgi?id=20016>)

368 AD: Alzheimer's disease; MCI: mild cognitive impairment; SCZ: schizophrenia; DM: diabetes
 369 mellitus; MDD: major depressive disorder; HTN: hypertension; ASD: autism spectrum disorder;
 370 CN: healthy control; PT: patient; *N*: number of participants. We decided not to harmonize
 371 cognitive scores from different studies.
 372

Trait (ICD-10 code or ID)	Sample size (CN/PT or <i>N</i>)	Site	Trait (ICD-10 code or ID)	Sample size (CN/PT or <i>N</i>)	Site
AD	1095/723	ADNI, PENN, & AIBL	Carpal tunnel syndrome (G560)	901/901	UKBB
MCI	1273/1095	ADNI, PENN, & AIBL	Lesion of ulnar nerve (G562)	104/104	UKBB
SCZ	1031/1094	PHENOM	Lesion of plantar nerve (G576)	163/163	UKBB
DM	1093/1093	UKBB	Angina pectoris (I20)	1535/1535	UKBB
MDD ^a	1476/1476	UKBB	Acute myocardial infarction (I21)	769/769	UKBB
HTN	934/887	ADNI, BLSA & CARDIA	Chronic ischaemic heart disease (I25)	2217/2217	UKBB

ASD	623/597	ABIDE	Pulmonary embolism (I20)	351/351	UKBB
Iron deficiency anemia (D50)	1012/1012	UKBB	Cardiomyopathy (I42)	116/116	UKBB
Vitamin B12 deficiency anemia (D50)	78/78	UKBB	Paroxysmal tachycardia (I47)	320/320	UKBB
Agranulocytosis (D70)	245/245	UKBB	Heart failure (I50)	436/436	UKBB
Thyrotoxicosis (E05)	205/205	UKBB	Cerebral infarction (I63)	291/291	UKBB
Vitamin D deficiency (E55)	180/180	UKBB	Vitamin B deficiency (E53)	130/130	UKBB
Obesity (E66)	1481/1481	UKBB	Hemiplegia (G81)	111/111	UKBB
Lipoprotein metabolism disorder (E78)	3880/3880	UKBB	Facial nerve disorders (G51)	95/95	UKBB
Mineral metabolism disorder (E83)	291/291	UKBB	Tower rearranging (21004)	8412	UKBB
Volume depletion	240/240	UKBB	Matrix pattern (6373)	8501	UKBB
Delirium	92/92	UKBB	TMT-A (6348)	8599	UKBB
Alcohol abuse	341/341	UKBB	TMT-B (6350)	8599	UKBB
Tobacco abuse	863/863	UKBB	DSST (23324)	8523	UKBB
Bipolar affective disorder	77/77	UKBB	Pairs matching (399)	20945	UKBB
Phobic anxiety disorder	84/84	UKBB	Numerical memory (4282)	9323	UKBB
Multiple sclerosis	109/109	UKBB	Prospective memory (4288)	19681	UKBB
Epilepsy	250/250	UKBB	Reaction time (20023)	21258	UKBB
Migraine	508/508	UKBB	Fluid intelligence (20016)	19184	UKBB
Sleep disorders	590/590	UKBB			

373
374

375 **eTable 3: Comparison of variants identified via MuSIC with other studies.** Using the AAL
376 atlas, we found (using the same data in the current study) that 269 independent significant SNPs
377 had 356 pairwise associations with 54 AAL brain regions. 230 out of the 269 SNPs matched with
378 the SNPs in MuSIC. Among the 39 unmatched SNPs, 15 SNPs were in linkage disequilibrium
379 (LD, $r^2 > 0.6$) with MuSIC SNPs (**Supplementary eFile 5**). As a second example, Zhao et al.¹¹
380 reported that 251 independent significant SNPs had 346 pairwise associations with 43 GM regions
381 using the Mindboggle atlas on the UKBB ($N=19,629$).¹² 129 of the 251 SNPs matched with SNPs
382 identified by MuSIC. Among these non-matching SNPs (127), 31 were in LD with MuSIC SNPs
383 (**Supplementary eFile 6**). Similarly, Elliot et al.¹³ ($N=8428$) discovered that 20 independent
384 significant SNPs had 58 pairwise associations with 52 GM regions from atlases in Freesurfer and
385 FSL software. Out of the 20 SNPs, 16 coincided with MuSIC SNPs. Among the four unmatched
386 SNPs, 1 SNP was in LD with MuSIC SNPs (**Supplementary eFile 7**). Note that the definition of
387 independent significant SNPs or genomic loci might slightly differ between studies.

Study/Atlas	Identified genomic loci	Matched loci	Loci in LD	Novel loci	Database	Sample size	Ancestry
MuSIC	915	NA	NA	NA	UKBB	18,052	European
AAL	218	162	13	740	UKBB	18,052	European
Zhao et al. ¹¹	251	73	14	828	UKBB	19,629	European
Elliot et al. ¹³	20	16	1	898	UKBB	8428	European
GWAS Catalog	NA	298	NA	617	NA	NA	NA

388
389

390 **eTable 4: Classification balanced accuracy for disease classification and effect size of these**
 391 **imaging signatures.**

392 Disease classification performance is presented using balanced accuracy. The mean and standard
 393 deviation are presented. Cohen's d was computed to compare the SPARE scores between groups.
 394 Multi-scale classification^a: All 2003 PSCs from multiple scales were fit into the classifier.
 395 Multi-scale classification^b: PSCs from all scales were fit into the classifier with a nested feature
 396 selection procedure (SVM-REF). The motivation is that PSCs from different scales are
 397 hierarchical and correlated. The nested feature selection can select the features most relevant to
 398 the specific task. We avoided any statistical comparison of the performance of machine learning
 399 models because available statistical tests are liberal and often lead to false-positive conclusions
 400 due to the complexity of the cross-validation procedure.¹⁴

401 a): Classification results for all subjects in all sites using a nested CV procedure

PSC	AD	d	MCI	d	SCZ	d	DM	d	HTN	d	MDD	d	ASD	d
C32	0.78± 0.02	1.52	0.62± 0.02	0.59	0.55± 0.02	0.30	0.56± 0.02	0.35	0.55± 0.02	0.28	0.52± 0.02	0.16	0.50± 0.02	0.07
C64	0.81± 0.02	1.73	0.63± 0.02	0.66	0.57± 0.02	0.41	0.57± 0.02	0.40	0.56± 0.02	0.31	0.53± 0.02	0.17	0.53± 0.02	0.19
C128	0.82± 0.02	1.82	0.65± 0.02	0.76	0.59± 0.02	0.47	0.56± 0.02	0.33	0.55± 0.02	0.30	0.52± 0.02	0.15	0.52± 0.02	0.15
C256	0.85± 0.02	2.08	0.66± 0.02	0.91	0.59± 0.02	0.50	0.56± 0.02	0.47	0.54± 0.02	0.31	0.51± 0.02	0.13	0.52± 0.02	0.16
C512	0.88± 0.02	2.34	0.67± 0.02	1.06	0.62± 0.02	0.62	0.57± 0.02	0.54	0.56± 0.02	0.42	0.52± 0.02	0.05	0.54± 0.02	0.24
C1024	0.90± 0.02	2.50	0.72± 0.02	1.12	0.65± 0.02	0.75	0.60± 0.02	0.59	0.59± 0.02	0.46	0.56± 0.02	0.13	0.55± 0.02	0.29
Multi-scale ^a	0.91± 0.02	2.54	0.72± 0.02	1.12	0.66± 0.02	0.77	0.61± 0.02	0.64	0.59± 0.02	0.47	0.55± 0.02	0.23	0.56± 0.02	0.30
Multi-scale ^b	0.92± 0.02	2.61	0.73± 0.02	1.13	0.67± 0.02	0.78	0.64± 0.02	0.67	0.61± 0.02	0.49	0.55± 0.02	0.26	0.58± 0.02	0.32
AAL	0.82± 0.02	1.81	0.66 ±0.02	0.75	0.59± 0.02	0.46	0.57± 0.02	0.32	0.57± 0.02	0.35	0.52± 0.02	0.08	0.52± 0.02	0.14
RAVENS	0.85± 0.02	2.04	0.64 ±0.02	0.74	0.60± 0.02	0.45	0.58± 0.02	0.33	0.55± 0.02	0.34	0.50± 0.02	0.05	0.54± 0.02	0.15

402 b): The classification results of the balanced accuracy (BA) from the test data in the nested CV
 403 and the independently left-out site for the task of AD vs. CN were assessed using all available
 404 multi-scale PSCs^a. Three sites, namely ADNI, AIBL, and PENN, were considered for this
 405 analysis. However, UKBB, BIOCARD, and BLSA data were excluded due to limited AD cases
 406 (eTable 1). Similarly, data from OASIS were excluded due to discrepancies in the diagnosis
 407 criteria for AD, as previously stated in our previous work⁷.

Left-out site	Test BA in CV	Test BA in the left-out site
ADNI	0.90±0.02	0.88±0.02
AIBL	0.88±0.02	0.95±0.02
PENN	0.90±0.02	0.95±0.02

409

410 **eTable 5:** 119 MUSE gray matter regions of interest.

411 L: Left hemisphere; R: Right hemisphere; ROI: region of interest.

MUSE ROI	MUSE ROI	MUSE ROI
Precentral gyrus (R)	Occipital fusiform gyrus (R)	Anterior insula (L)
Precentral gyrus (L)	Planum temporale (R)	Anterior orbital gyrus (R)
Accumbens area (R)	Cerebellar vermal lobules I-V	Anterior orbital gyrus (L)
Accumbens area (L)	Cerebellar vermal lobules VI-VII	Angular gyrus (R)
Amygdala (R)	Cerebellar vermal lobules VIII-X	Angular gyrus (L)
Amygdala (L)	Basal forebrain (R)	Calcarine cortex (R)
Occipital pole (L)	Basal forebrain (L)	Calcarine cortex (L)
Caudate (R)	Middle temporal gyrus (L)	Central operculum (R)
Caudate (L)	Occipital pole (R)	Central operculum (L)
Cerebellum exterior (R)	Planum temporale (L)	Cuneus (R)
Cerebellum exterior (L)	Parietal operculum (L)	Cuneus (L)
Planum polare (L)	Postcentral gyrus (R)	Entorhinal area (R)
Middle temporal gyrus (R)	Postcentral gyrus (L)	Entorhinal area (L)
Hippocampus (R)	Posterior orbital gyrus (R)	Frontal operculum (R)
Hippocampus (L)	Temporal pole (R)	Frontal operculum (L)
Precentral gyrus medial segment (R)	Temporal pole (L)	Frontal pole (R)
Precentral gyrus medial segment (L)	Triangular part of the inferior frontal gyrus (R)	Frontal pole (L)
Superior frontal gyrus medial segment (R)	Triangular part of the inferior frontal gyrus (L)	Fusiform gyrus (R)
Superior frontal gyrus medial segment (L)	Transverse temporal gyrus (R)	Fusiform gyrus (L)
Pallidum (R)	Superior frontal gyrus medial segment (L)	Gyrus rectus (R)
Pallidum (L)	Planum polare (R)	Gyrus rectus (L)
Putamen (R)	Transverse temporal gyrus (L)	Inferior occipital gyrus (R)
Putamen (L)	Anterior cingulate gyrus (R)	Inferior occipital gyrus (L)
Thalamus proper (R)	Anterior cingulate gyrus (L)	Inferior temporal gyrus (R)
Thalamus proper (L)	Anterior insula (R)	Inferior temporal gyrus (L)
Lingual gyrus (R)	Occipital fusiform gyrus (L)	Subcallosal area (R)
Lingual gyrus (L)	Opercular part of inferior frontal gyrus (R)	Subcallosal area (L)
Lateral orbital gyrus (R)	Opercular part of inferior frontal gyrus (L)	Superior frontal gyrus (R)
Lateral orbital gyrus (L)	Orbital part of inferior frontal gyrus (R)	Superior frontal gyrus (L)
Middle cingulate gyrus (R)	Orbital part of inferior frontal gyrus (L)	Supplementary motor cortex (R)
Middle cingulate gyrus (L)	Posterior cingulate gyrus (R)	Supplementary motor cortex (L)
Medial frontal cortex (R)	Posterior cingulate gyrus (L)	Supramarginal gyrus (R)
Medial frontal cortex (L)	Precuneus (R)	Supramarginal gyrus (L)
Middle frontal gyrus (R)	Precuneus (L)	Superior occipital gyrus (R)
Middle frontal gyrus (L)	Parahippocampal gyrus (R)	Superior occipital gyrus (L)
Middle occipital gyrus (R)	Parahippocampal gyrus (L)	Superior parietal lobule (R)
Middle occipital gyrus (L)	Posterior insula (R)	Superior parietal lobule (L)
Medial orbital gyrus (R)	Posterior insula (L)	Superior temporal gyrus (R)
Medial orbital gyrus (L)	Parietal operculum (R)	Superior temporal gyrus (L)
Superior frontal gyrus medial segment (R)	Posterior orbital gyrus (L)	

412

413 **eAlgorithm 1:** Algorithm for sopNMF.
 414 The source code of the Python implementation of sopNMF is available here:
 415 <https://github.com/anbai106/SOPNMF>

Algorithm 1: sopNMF

- **Input:** maximum number of epochs e , number of component C or r , batch size b , early stopping criteria θ (i.e., the loss without decreasing for a certain epochs) ;
- **Output:** $\mathbf{W} \in \mathbb{R}^{d \times r}$, $\mathbf{H} \in \mathbb{R}^{r \times n}$;
- **Initialization:** \mathbf{W} ;

```

if not  $\theta$  or epoch  $\neq e$  then
  for  $p \leftarrow 0$  to  $e$  do
    for  $i \leftarrow 0$  to  $t$  do
      Read mini-batch  $\mathbf{X}_{bi}$ 
      Update  $\mathbf{W}_{i+1}$  via Eq. 2
    end
     $loss = \sum_{i=1}^{\lfloor \frac{n}{b} \rfloor} \|\mathbf{X}_{bi} - \mathbf{W}\mathbf{W}^T \mathbf{X}_{bi}\|_F^2$  (Eq.3)
    if loss in  $\theta$  then
      Stop
    else
      Shuffle  $\mathbf{X}$ 
      Continue
    end
  end
else
  Stop
end

```

416
 417
 418

419 **References**

- 420
- 421 1. Shalev-Shwartz, S., Singer, Y. & Ng, A. Y. Online and batch learning of pseudo-metrics. in
- 422 *Proceedings of the twenty-first international conference on Machine learning* 94
- 423 (Association for Computing Machinery, 2004). doi:10.1145/1015330.1015376.
- 424 2. Kuhn, H. W. The Hungarian method for the assignment problem. *Naval Research Logistics*
- 425 *Quarterly* **2**, 83–97 (1955).
- 426 3. Pomponio, R. *et al.* Harmonization of large MRI datasets for the analysis of brain imaging
- 427 patterns throughout the lifespan. *Neuroimage* **208**, 116450 (2020).
- 428 4. Watanabe, K., Taskesen, E., van Bochoven, A. & Posthuma, D. Functional mapping and
- 429 annotation of genetic associations with FUMA. *Nat Commun* **8**, 1826 (2017).
- 430 5. Purcell, S. *et al.* PLINK: A Tool Set for Whole-Genome Association and Population-Based
- 431 Linkage Analyses. *Am J Hum Genet* **81**, 559–575 (2007).
- 432 6. Samper-González, J. *et al.* Reproducible evaluation of classification methods in
- 433 Alzheimer’s disease: Framework and application to MRI and PET data. *NeuroImage* **183**,
- 434 504–521 (2018).
- 435 7. Wen, J. *et al.* Convolutional neural networks for classification of Alzheimer’s disease:
- 436 Overview and reproducible evaluation. *Medical Image Analysis* **63**, 101694 (2020).
- 437 8. Wen, J. *et al.* Reproducible Evaluation of Diffusion MRI Features for Automatic
- 438 Classification of Patients with Alzheimer’s Disease. *Neuroinformatics* **19**, 57–78 (2021).
- 439 9. Stasinopoulos, D. M. & Rigby, R. A. Generalized Additive Models for Location Scale and
- 440 Shape (GAMLSS) in R. *Journal of Statistical Software* **23**, 1–46 (2008).

- 441 10. Wen, J. *et al.* Characterizing Heterogeneity in Neuroimaging, Cognition, Clinical
442 Symptoms, and Genetics Among Patients With Late-Life Depression. *JAMA Psychiatry*
443 (2022) doi:10.1001/jamapsychiatry.2022.0020.
- 444 11. Zhao, B. *et al.* Genome-wide association analysis of 19,629 individuals identifies variants
445 influencing regional brain volumes and refines their genetic co-architecture with cognitive
446 and mental health traits. *Nat Genet* **51**, 1637–1644 (2019).
- 447 12. Klein, A. & Tourville, J. 101 Labeled Brain Images and a Consistent Human Cortical
448 Labeling Protocol. *Frontiers in Neuroscience* **6**, 171 (2012).
- 449 13. Elliott, L. T. *et al.* Genome-wide association studies of brain imaging phenotypes in UK
450 Biobank. *Nature* **562**, 210–216 (2018).
- 451 14. Nadeau, C. & Bengio, Y. Inference for the Generalization Error. in *Advances in Neural*
452 *Information Processing Systems 12* (eds. Solla, S. A., Leen, T. K. & Müller, K.) 307–313
453 (MIT Press, 2000).
- 454